

PHYSICAL REVIEW B

SOLID STATE

THIRD SERIES, VOL. 5, No. 1

1 JANUARY 1972

Channeling in Iron and Lattice Location of Implanted Xenon

L. C. Feldman* and D. E. Murnick

Bell Laboratories, Murray Hill, New Jersey 07974

(Received 19 July 1971)

We have studied heavy-ion (^4He , ^{12}C , ^{14}N) channeling in carefully prepared iron single crystals. Angular distributions and critical angles in good agreement with the Lindhard theory were obtained. $^{131,132}\text{Xe}$ was implanted into the iron crystal at 100 or 200 keV in a random direction at doses of $(1-100) \times 10^{14}$ atoms/cm². In all cases, some radiation damage was evident from an increase in the minimum channeling yield. Typically $(50 \pm 10)\%$ of implanted Xe was found to be at lattice sites at low doses, while most of the atoms were not substitutional at higher doses. Annealing at 450 °C reduced the substitutional fraction; annealing at 300 °C did not. These data are compared with Mössbauer-effect studies of hyperfine fields on Cs in iron.

I. INTRODUCTION

Hyperfine interactions on dilute impurities in iron metal have been studied in great detail in recent years.¹⁻³ Nuclear-magnetic-resonance, Mössbauer-effect, nuclear-orientation, and perturbed-angular-correlation experiments have all been concerned with the interaction of nuclear magnetic moments with the large effective hyperfine fields induced at impurity nuclei in the ferromagnetic lattice. For several systems, particularly those prepared by ion-implantation techniques, the hyperfine interaction has been found to be nonunique and to vary with sample preparation procedures.⁴

Indirect evidence as to the physical state of implanted atoms can be obtained from the hyperfine-interaction data itself. More than one frequency component, line broadening, and irreproducibility are examples of experimental effects attributed to lattice locations and/or radiation damage effects. Channeling, however, allows a direct, relatively unambiguous measure of impurity lattice site and certain types of radiation damage. The correlation of channeling results with indirect hyperfine-interaction results may prove or disprove relationships which are now tentatively inferred (e. g., high field implies substitutional ion). Furthermore, such data are important for an understanding of all hyperfine-interaction experiments on implanted samples, and may shed light on the complex polarization phenomena inducing the large hyperfine fields mea-

sured.

In this paper, experiments on heavy-ion channeling in carefully prepared iron single crystals are reported. The lattice location of, and radiation damage induced by, implantation of xenon into the crystal were studied as a function of dose and annealing temperature; and the results compared with Mössbauer-effect experiments on radioactive ^{133}Xe implanted into iron.⁵ Xenon, being a rare gas, is, in a sense, a very special case, but as is described below, quite sensitive to "implantation effects." Furthermore, the careful and complete Mössbauer-effect experiments of de Waard *et al.* using xenon implanted into iron allow a complete comparison of lattice location with hyperfine-interaction results.

The channeling literature and theory of lattice-location experiments utilizing scattering yields of heavy projectiles in aligned and random directions need not be reviewed here.^{6,7} Detailed channeling studies via backscattering from pure iron crystals have not previously been reported. At least two lattice-location experiments in iron have been reported previously.^{8,9} During the course of this work additional studies have begun at our laboratory and elsewhere so that some tentative statements may now be made about systematics of impurity location of atoms implanted into iron.

In this paper, our experimental procedure and apparatus for channeling and ion implantation are described. Results of channeling experiments in iron with ^4He , ^{12}C , and ^{14}N projectiles are reviewed.

Xenon-implantation effects at different doses and annealing treatments are described, and the results of lattice-location experiments are discussed and tabulated. Conclusions from these investigations relevant to the hyperfine-interaction studies are also presented.

II. EXPERIMENTAL PROCEDURE AND APPARATUS

Good single crystals of pure iron are difficult to grow because of the phase changes at 800 and 1100 °C to β - and γ -iron. For these investigations we used bcc α -iron crystals grown by the float-zone process in the form of slabs by Materials Research Ltd., Cambridge, England.

The iron samples were carefully mechanically polished and electropolished to assure good and clean surfaces prior to use. Normal care was observed in handling, though the crystals were exposed to air for periods ranging from a few minutes to a few hours prior to being mounted on the goniometer and placed in the vacuum chamber.

Figure 1 is a schematic drawing of the ion-implantation and channeling facility. A 2-MeV Van de Graaff accelerator is used to accelerate helium, carbon, oxygen, or nitrogen ions which are collimated to 0.015° by two 1-mm circular collimators and passed through an annular surface-barrier particle detector onto the iron crystal. The sample crystal may be rotated and/or tilted, allowing a determination of its channeling properties from the angular dependence of the Rutherford backscatter yield.

The detector subtends a partial cone of 174° to 178° and has energy resolution of approximately 25 keV. The use of an annular detector minimizes the possibility of blocking effects, i. e., anomalous intensity variations occurring near high-symmetry crystalline directions parallel to the emission di-

rection of the scattered particle. The usual procedure in these experiments was to observe the channeling properties of a polished virgin crystal, then to implant, and finally to observe the post-implant channeling of the iron-xenon system.

For the implant, the first collimator is changed to 1-cm diameter and the second collimator and annular detector are removed. The heavy-ion beam is swept over an area of about 0.4 cm² by deflecting plates to ensure a uniform doping. All the implants described in this paper were done with the substrate at room temperature, with 100- or 200-keV singly charged ^{131,132}Xe beams in doses from about 1 × 10¹⁴ to 1 × 10¹⁶/cm². Surrounding the sample in the goniometer is a thermally and electrically insulated copper cup which acts as a cold trap to reduce surface contamination during the experiment and as a secondary electron suppressor to assure accurate dose measurements and beam normalizations. The amount of Xe implanted is also checked by evaluating the scattering intensity in the xenon backscatter peak.

III. CHANNELING IN IRON

Figure 2 shows typical angular distributions of heavy-ion backscatter intensity for scattering occurring near the iron crystal surface as a function of angle between the beam and a crystal axis. The yield is normalized to 1.0 at an angle far from the symmetry direction. The minimum yield, χ_{\min} , is ~0.025 for 2-MeV He in the $\langle 100 \rangle$ direction and 0.03 for 1.7-MeV N in the $\langle 111 \rangle$ direction. The $\langle 100 \rangle$ minimum yield is in good agreement with the calculations of Barrett¹⁰ while the $\langle 111 \rangle$ measurement is approximately a factor of 1.5 higher than the Barrett prediction. This may be due to higher multiple scattering in the effectively thicker surface region of the tilted crystal. The average

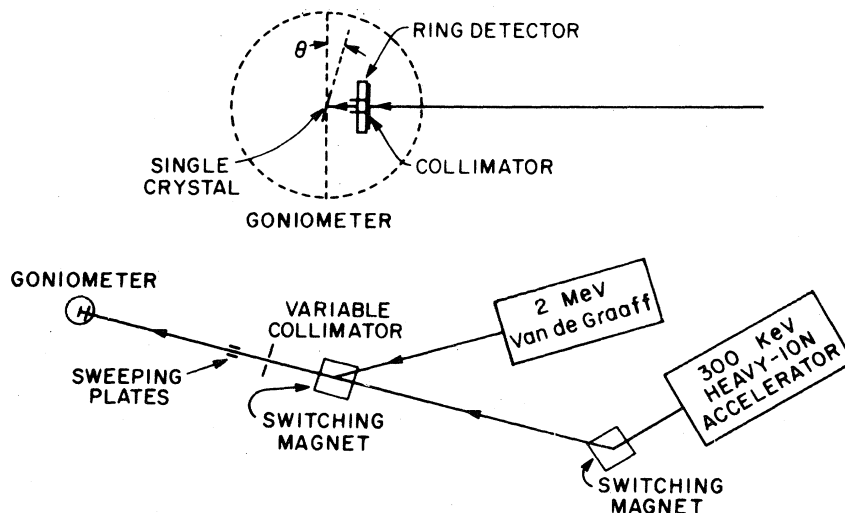


FIG. 1. Schematic of experimental facility.

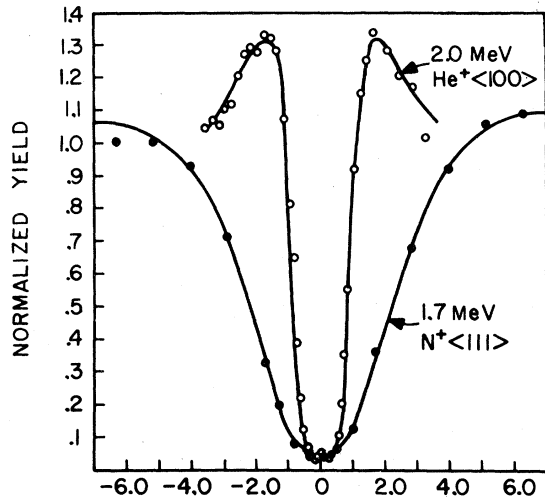


FIG. 2. Backscattered axial yields for 2.0-MeV He incident along the $\langle 100 \rangle$ axis and 1.7-MeV N incident along the $\langle 111 \rangle$ axis.

square amplitude of thermal vibrations is taken as $9.6 \times 10^{-3} \text{ \AA}^2$ at 300 °K for this comparison. The angular widths of the pattern are about 0.85° and 2.18° for He and N, respectively, and agree to within 10% with the theoretical expression:

$$\psi_c = \left(\frac{2Z_1 Z_2 e^2}{Ed} \right)^{1/2},$$

where Z_1 and Z_2 are the beam and host atomic numbers, d is the atomic spacing along the string, and E is the beam energy.

A typical energy spectrum of backscattered 2.0-MeV He incident parallel to the $\langle 111 \rangle$ axis is shown in Fig. 3 with a normalized spectrum for the beam incident far from the axial direction. In the channeled spectrum there is a peak evident at about 1.5 MeV corresponding to scattering from the surface of the crystal. There is also a slight peak at about 0.4 MeV corresponding to scattering from surface oxygen. The area under the iron peak corresponds to a layer of 2×10^{16} Fe atoms/cm² or, assuming that it is primarily a layer of iron oxide, corresponds to about 25 Å of Fe₂O₃. Bøgh,⁹ using the double alignment technique for greater sensitivity to the oxygen and iron surface peak, has verified the stoichiometry, Fe₂O₃, as well as a thickness of ~30 Å for their crystal. The thickness of this layer points out the necessity for high-enough-energy ion implantation in hyperfine-interaction experiments to ensure that the ion comes to rest in iron and not in the oxide layer. The ratio of the yield directly below the surface peak to the yield of the random at the same energy (i.e., same depth) is the best measure of minimum yield. For the case shown here, we measure minimum yields of 0.028, 0.030, and 0.054 for the $\langle 111 \rangle$, $\langle 100 \rangle$,

and $\langle 110 \rangle$ directions, respectively. Qualitatively this obeys the d dependence of χ_{\min} predicted by Lindhard.

The aligned yield increases faster, at greater depths, than the normal yield due to dechanneling effects. The half-thickness for particle escape of 2.0-MeV He is ~14 μm in the $\langle 111 \rangle$ direction. It is possible that a high density of light interstitial impurities which would not be detected in the backscatter energy spectrum would increase the rate of dechanneling.

IV. XENON IMPLANTATION

The stable xenon isotopes of mass numbers 128–132 and 134 and 136 could be separated in the output beam of the ion-implantation mass-separator apparatus. For these experiments, the Xe¹³¹ (natural abundance 21.24%) and Xe¹³² (natural abundance 26.93%) components were focused to a spot, and using the beam-sweeping device described elsewhere, uniform large-area implants were obtained. Singly charged Xe beams of about 1–3 μA were integrated on the electrically isolated crystal until the desired impurity dose was obtained. The dose was later checked by the Rutherford backscatter yield of 2-MeV He or N. Agreement within about a factor of 2 was always obtained. The xenon doses quoted below, $(1-100) \times 10^{14}/\text{cm}^2$, were deter-

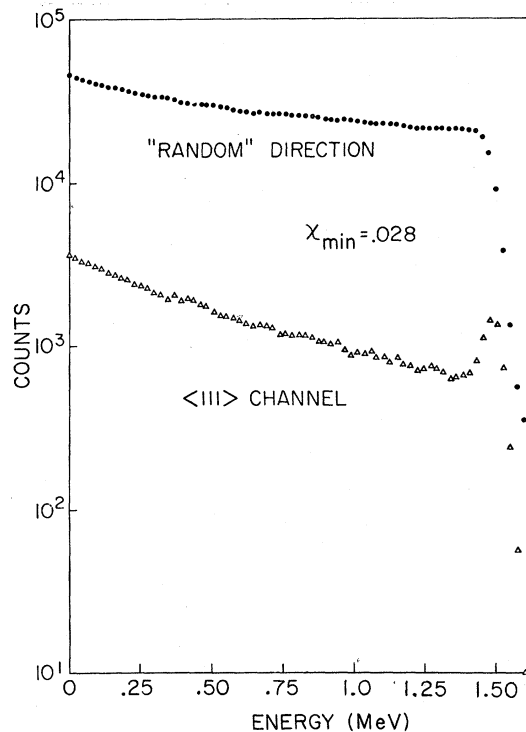


FIG. 3. Normalized backscatter energy spectra for 2-MeV He incident parallel to the $\langle 111 \rangle$ axis of a clean iron crystal and incident in a nonchanneling direction.

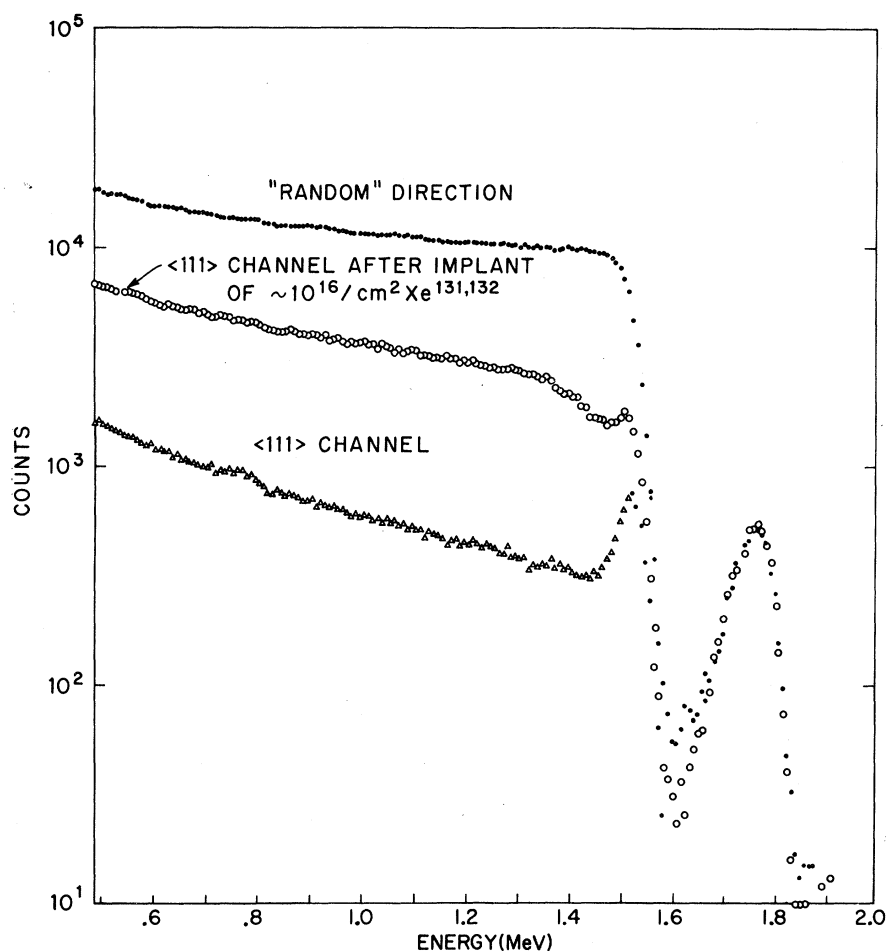


FIG. 4. Normalized backscattered 2.0-MeV He spectra pre- and post-high-dose implant of Xe into iron crystal. The high-energy peak is depressed for lower-dose implants, and the change in minimum yield is less pronounced.

mined from the backscatter yield.

The range of 200-keV Xe in iron is about 300 \AA with a range straggling ΔR approximately 100 \AA .¹¹ For 100-keV ions the comparable figures are 170 and 60 \AA , respectively. The volume concentrations tabulated below are calculated with the simple model of a uniform doping in a layer $R - \Delta R$ to $R + \Delta R$. Clearly, equivalent doses at lower implant energies lead to higher volume concentrations. Low implant energies must also be avoided to ensure against stopping in the oxide layer. For average iron samples our data indicate that $R - 2\Delta R$ should be greater than $\sim 30 \text{ \AA}$, the typical oxide thickness. This condition is particularly important for radioactive implants, when subsequent γ -ray spectroscopy (as with the Mössbauer effect) yields no depth information.

Figure 4 shows the scattering yield of 2.0-MeV He pre- and post-implant of $2 \times 10^{16} \text{ atoms/cm}^2$ xenon at 200 keV. The channeling spectra for the $\langle 111 \rangle$ axis are shown. The extraordinarily high dose is chosen here for illustrative purposes as implantation effects were not as immediately appar-

ent for the lower doses. Several conclusions can be drawn from the figure. First, one sees a large increase in the channeling minimum-yield post-implant. The increase can be attributed to scattering from interstitial iron atoms displaced during the implantation. In this case the number of such atoms corresponds to about $1.6 \times 10^{22}/\text{cm}^3$ in the implanted region. The shape of the post-implant spectrum may also be due to strain in the crystal, particularly in this high-dose case. For similar implants of about $10^{14} \text{ atoms/cm}^2$, the increase in minimum yield was only a factor of 1.5–2. In the high-dose case one also sees evidence of damage corresponding to the maximum in nuclear stopping as the implanted ions slowed down. The depth of the damage maximum should be less than the range of the implanted xenon. It should be noted that the depth resolution is about 180 \AA in this case. The total damage is far less than would be expected from the Kinchin-Pease formula¹² or is observed for similar doses in a semiconductor due to self-annealing in the metal. Higher-temperature implants, yet to be studied, might lead to considera-

TABLE I. Summary of experimental results.

Xe dose	Concentration at. %	Channel	Xe backscatter yield	Substitutional fraction	High-field fraction
1×10^{14}	0.08	$\langle 110 \rangle$	0.67 ± 0.20	0.39 ± 0.15	0.55
		$\langle 100 \rangle$	0.59 ± 0.19		
1×10^{14}	0.13	$\langle 111 \rangle$	0.69 ± 0.13	0.32 ± 0.15	0.74
		$\langle 110 \rangle$	0.67 ± 0.20		
2.3×10^{14}	0.31	$\langle 111 \rangle$	0.52 ± 0.06	0.49 ± 0.05	0.61
		$\langle 100 \rangle$	0.49 ± 0.06		
2.3×10^{14}	Post-450 °C anneal	$\langle 111 \rangle$	0.95 ± 0.05	0.09 ± 0.05	<0.10
		$\langle 100 \rangle$	0.88 ± 0.05		
2.5×10^{14}	0.34	$\langle 100 \rangle$	0.53 ± 0.10	0.47 ± 0.10	0.61
3.8×10^{14}	0.51	$\langle 111 \rangle$	0.59 ± 0.11	0.45 ± 0.10	
		$\langle 100 \rangle$	0.55 ± 0.12		
1×10^{16}	8.4	$\langle 111 \rangle$	0.80 ± 0.03		
		$\langle 110 \rangle$	0.87 ± 0.03	0.16 ± 0.03	0.22
		$\langle 100 \rangle$	0.84 ± 0.03		

bly less damage in analogy with the semiconductor case.

V. LATTICE-LOCATION STUDIES

de Waard and collaborators have studied the Mössbauer effect of ^{133}Cs in iron produced by the β decay of radioactive ^{133}Xe which was implanted at 50 keV into iron foils.⁵ Briefly, the results of the Mössbauer-effect experiments were as follows:

(i) Two components to the hyperfine spectra were observed; a high-field large isomer shift site ($H_{\text{int}} = 273$ kOe, $\sigma = 1.1$ mm/sec) and a low-field low isomer shift site ($H_{\text{int}} < 30$ kOe, $\sigma \approx 0.3$ mm/sec); (ii) the high-field component was considerably reduced after annealing at about 400 °C; and (iii) single-crystal iron behaved like polycrystalline iron.

From these results, as well as the temperature dependence of the recoil-free fraction, the percentage of Cs atoms at high-field sites was deduced to be about 60% and assumed to be substitutional.

Figure 5 illustrates the bcc iron lattice and displays two possible stable interstitial sites. The

face-center site of octahedral symmetry is equivalent to a site on the $\langle 100 \rangle$ axis and hence would appear substitutional for channeling in that direction as well as the $\langle 110 \rangle$, but would appear interstitial for channeling along the $\langle 111 \rangle$ axis. ("Flux-peaking"¹³ effects are not considered in this paper. If some of the Xe were at "flux-peaking sites," the quantitative interpretation of our data would be altered. However, the good agreement between different directions tends to indicate that such sites are not occupied.) The site of tetrahedral symmetry is possibly more stable for a heavy ion and would look interstitial for all major axes but substitutional along the $\langle 120 \rangle$ direction, for which the sensitivity of these experiments is low. Table I summarizes the results of our channeling lattice-location experiments. For increased sensitivity at low doses the probing beam was 2.0-MeV C^{12} . The minimum yield for carbon was not significantly greater than for helium, but the better energy

TABLE II. Summary of channeling information on implanted impurity sites in iron.

Impurity	Dose	Implantation energy (keV)	Approximate substitutional fraction	Ref.
Lu	3×10^{15}	40	0.40	a
Sn	2×10^{16}	150	0.85	b
Yb	10^{15}	60	0.50	c
Xe	10^{14} – 10^{16}	100–200	0.45	d
Pb	2×10^{14}	100	0.82	e
Bi	2×10^{14}	100	0.79	e
Tl	2×10^{14}	170	0.84	e

^aReference 8.

^bReference 9.

^cB. Deutch, in Ref. 3.

^dThis work.

^eL. C. Feldman and E. N. Kaufmann (unpublished).

STABLE IMPURITY SITES IN bcc IRON

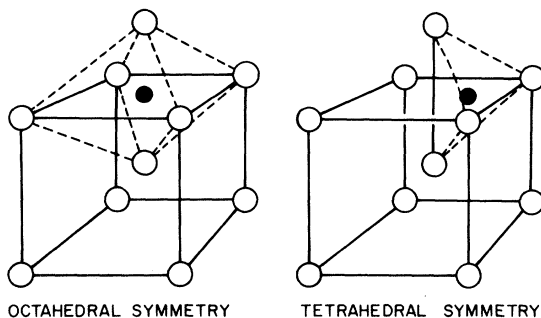


FIG. 5. Possible stable impurity sites in body-centered-cubic α -iron.

separation between surface iron and xenon scattering was considerable because of increased elastic-energy loss. In addition, the higher specific-energy loss for carbon in iron enhanced the depth resolution somewhat, part of the intrinsic gain being lost by the poorer detector resolution of ~ 50 keV for carbon.

The substitutional fraction (F_{sub}) associated with each axial direction was determined from the integrated xenon peak in random and aligned directions using the relationship

$$F_{\text{sub}} = \frac{1 - Y_C/Y_R}{1 - \chi_{\text{min}}},$$

where Y_C , Y_R are the relative backscatter yields in channeling and random directions and $1 - \chi_{\text{min}}$ corrects for the fraction of the beam nonchanneled.

There were no significant differences in $Y_{\langle 111 \rangle}$ and $Y_{\langle 100 \rangle}$ or $Y_{\langle 110 \rangle}$ for the same dose, indicating that the face-center site is not a favored interstitial. Limited data for the $\langle 120 \rangle$ axis indicate some enhancement for the tetrahedral site, but no quantitative results were obtained due to low sensitivity.

The 0.51% sample was annealed at 300 °C for 5 min with no change in substitutional fraction. A similar anneal at 450 °C for the 0.31% sample showed a substantial decrease in substitutional xenon, however, indicating the instability of the substitutional site.

Column five of the table is an approximate comparison with the Mössbauer-effect data; "high-field fraction" having tentatively been identified with substitutional site. The agreement of the high-dose and post-anneal results indicates that the tentative identification is indeed correct. The lack of exact agreement between substitutional fraction and high-field fraction may be due to any of several reasons. The experiments were done on different

samples, and both groups noticed some variation from sample to sample. Also, the Mössbauer results depend on a derived recoil-free-fraction ratio and assume only two sites.

Note added in proof. A reanalysis of the Mössbauer results (de Waard, private communication) utilizing three components yields better agreement between the high field and substitutional fractions.

VI. SUMMARY

Xenon implanted into carefully prepared iron crystals at 100–200 keV yielding volume concentrations less than 1% has been shown, via channeling, to be ≈ 35 to 50% substitutional. The favored interstitial site is not the face center, and the substitutional fraction decreases above about 400 °C. From comparison with ^{133}Cs Mössbauer data the high-internal-field site is correlated with the substitutional site.

From these and other hyperfine-interaction experiments on implanted samples, it is clear that more information than is usually obtained from one experiment is necessary for valid hyperfine-interaction-data interpretation. In particular, the substitutional fraction, which can be obtained by the channeling technique, should be determined. Table II is a list of known lattice locations in iron experiments to date for various impurities. The substitutional fraction is seen to vary from almost 1.0 to less than 0.1 after annealing. Until definite systematics are determined, each case must separately be investigated.

ACKNOWLEDGMENTS

Helpful and informative discussions with H. de Waard are appreciated. We thank W. M. Augustyniak, J. W. Rodgers, and W. F. Flood for considerable technical assistance.

*Currently on leave of absence at University of Aarhus, Aarhus, Denmark.

¹*Hyperfine Structure and Nuclear Radiations*, edited by E. Matthias and D. Shirley (North-Holland, Amsterdam, 1968).

²Proc. Roy. Soc. (London) **A311** (1969).

³*Hyperfine Interactions in Excited Nuclei*, edited by G. Goldring and R. Kalish (Gordon and Breach, New York, 1971).

⁴P. G. E. Reid, M. Scott, N. J. Stone, D. Spanjaard, and H. Bernas, Phys. Letters **25A**, 396 (1967).

⁵H. de Waard and S. A. Drentje, Proc. Roy. Soc. (London) **A311**, 139 (1969); H. de Waard, P. Schurer, P. Inia, L. Niesen, and Y. K. Agarwal, in Ref. 3, p. 89.

⁶J. Lindhard, Kgl. Danske Videnskab. Selskab, Mat.-Fys. Medd. **34**, No. 14 (1965).

⁷The technique of lattice location via channeling is most completely described by J. W. Mayer, L. Eriksson, and J. A. Davies, *Ion Implantation in Semiconductors* (Academic, New York, 1970).

⁸M. Schmorak and E. Bøgh, in Ref. 1, p. 712.

⁹E. Bøgh, Proc. Roy. Soc. (London) **A311**, 35 (1969).

¹⁰J. Barrett, Phys. Rev. **B3**, 1527 (1971).

¹¹H. Schiott, Radiat. Eff. **6**, 107 (1970).

¹²P. Sigmund, Radiat. Eff. **1**, 15 (1969).

¹³J. U. Andersen, O. Andreasen, J. A. Davies, and E. Uggerhøj, Radiat. Eff. **7**, 25 (1971); B. Domeij, G. Fladda, and N. G. E. Johansson, *ibid.* **6**, 155 (1970).